

The influence of a kinematically cold young component on disc–halo decompositions in spiral galaxies: insights from solar neighbourhood K-giants

S. Aniyán,^{1★} K. C. Freeman,^{1★} O. E. Gerhard,² M. Arnaboldi^{3,4} and C. Flynn⁵

¹Research School of Astronomy & Astrophysics, Australian National University, via Cotter Road, Weston, ACT 2611, Australia

²Max-Planck-Institut für Extraterrestrische Physik, Giessenbachstrasse, D-85741 Garching, Germany

³European Southern Observatory, Karl-Schwarzschild Str. 2, D-85748 Garching, Germany

⁴INAF, Osservatorio Astronomico di Torino, Strada Osservatorio 20, I-10025 Pino Torinese, Italy

⁵Centre for Astrophysics and Supercomputing, Swinburne University, Hawthorn, VIC 3122, Australia

Accepted 2015 November 18. Received 2015 November 18; in original form 2015 September 11

ABSTRACT

In decomposing the H I rotation curves of disc galaxies, it is necessary to break a degeneracy between the gravitational fields of the disc and the dark halo by estimating the disc surface density. This is done by combining measurements of the vertical velocity dispersion of the disc with the disc scaleheight. The vertical velocity dispersion of the discs is measured from absorption lines (near the *V* band) of near-face-on spiral galaxies, with the light coming from a mixed population of giants of all ages. However, the scaleheights for these galaxies are estimated statistically from near-IR surface photometry of edge-on galaxies. The scaleheight estimate is therefore dominated by a population of older (>2 Gyr) red giants. In this paper, we demonstrate the importance of measuring the velocity dispersion for the same older population of stars that is used to estimate the vertical scaleheight. We present an analysis of the vertical kinematics of K-giants in the solar vicinity. We find the vertical velocity distribution best fitted by two components with dispersions of $9.6 \pm 0.5 \text{ km s}^{-1}$ and $18.6 \pm 1.0 \text{ km s}^{-1}$, which we interpret as the dispersions of the young and old disc populations, respectively. Combining the (single) measured velocity dispersion of the total young + old disc population ($13.0 \pm 0.1 \text{ km s}^{-1}$) with the scaleheight estimated for the older population would underestimate the disc surface density by a factor of ~ 2 . Such a disc would have a peak rotational velocity that is only 70 per cent of that for the maximal disc, thus making it appear submaximal.

Key words: Galaxy: disc–Galaxy: kinematics and dynamics–solar neighbourhood–galaxies: haloes.

1 INTRODUCTION

Galactic rotation curves are currently the best way to measure parameters for dark haloes of spiral galaxies, such as their typical scale densities and scalelengths. These quantities are interesting in themselves but they are also cosmologically significant, because the densities and scale radii of dark haloes follow well-defined scaling laws which can be used to measure the redshift of assembly of haloes of different masses (Macciò et al. 2013; Kormendy & Freeman 2014).

The density profiles of the dark haloes of spiral galaxies can be measured by decomposing their 21-cm rotation curves into the contributions from the disc and the dark halo. In the decomposition process, the shape of the disc’s contribution to the rotation curve

is calculated from the radial light distribution of the disc. It is then scaled according to the adopted mass-to-light ratio (*M/L*) of the disc. For the solar neighbourhood, the *M/L* values for the solar neighbourhood can be determined directly from star counts: e.g. Just et al. (2015) for the near-IR and Flynn et al. (2006) for optical bands. They find $M/L \sim 1.5, 1.2$ and $0.34 (M/L)_{\odot}$ in the *V*, *I* and *K* band, respectively. These values cannot be universally applied to other Galactic regions and other discs because *M/L* depends on the local star formation history. The stellar *M/L* values for external discs are still uncertain. As the adopted *M/L* of the disc is increased, the disc contributes increasingly more to the rotation curve, and the resulting halo becomes less dense and has a longer scalelength. The adopted *M/L* for the disc is critical to the outcome. The *M/L* can be estimated from the rotation curve itself, but this suffers from the well-known degeneracy between the contributions from the disc and the dark halo (van Albada et al. 1985).

The stellar *M/L* can in principle be estimated from stellar population synthesis (SPS) models (e.g. Bell & de Jong 2001) but this

* E-mail: suryashree.anayan@anu.edu.au (SA); kenneth.freeman@anu.edu.au (KCF)

remains insecure as it requires several significant assumptions such as the star formation and chemical enrichment history, the stellar initial mass function (IMF), accurate accounting of late phases of stellar evolution (e.g. Maraston 2005) and the internal dust absorption (Tully & Fouqué 1985).

To break the disc–halo degeneracy, the vertical velocity dispersion of stars in the discs can be used to measure the surface mass density of the disc (e.g. Bottema 1997; Herrmann et al. 2008). From the 1D Jeans equation in the vertical direction, the vertical velocity dispersion σ_z (integrated vertically through the disc) and the vertical disc scaleheight h together give the surface mass density Σ of the disc from the simple relation:

$$\Sigma = f\sigma_z^2/Gh, \quad (1)$$

where G is the gravitational constant and f is a geometric factor that depends weakly on the adopted vertical structure of the disc. The surface brightness of the disc and the surface mass density (Σ from equation 1) together give the M/L of the disc. The factor $f = 2/3\pi$ for a vertically exponential disc, and $f = 1/2\pi$ for a vertically isothermal disc (van der Kruit & Freeman 2011). The velocity dispersion σ_z is measured from spectra of the integrated light of the disc in relatively face-on galaxies. These observations are difficult because high-resolution spectra of low surface brightness discs are required to measure the small dispersions (for the old disc near the sun, $\sigma_z \sim 20 \text{ km s}^{-1}$). The other parameter, the disc scaleheight h , is typically about 250 pc, but cannot be measured directly for these face-on galaxies. It has to be estimated statistically from similar galaxies, seen edge-on, using the relation between scaleheight and absolute magnitude or circular velocity that has been measured for samples of edge-on galaxies. Yoachim & Dalcanton (2006) show the correlation of the scaleheights of the thin and thick disc with circular velocity of edge-on disc galaxies using R -band data. Similarly, Kregel, van der Kruit & Freeman (2005) did I -band studies of edge-on disc galaxies and show correlations between the scaleheight and intrinsic properties of the galaxy such as its surface brightness. van der Kruit & Freeman (1984), Bottema, van der Kruit & Freeman (1987) and Bershady et al. (2010) have used this method and find that the disc M/L is relatively low and the discs are submaximal.¹ Bershady et al. (2011) find that the dynamical stellar M/L obtained is about three times lower than the M/L from maximum disc hypothesis.

Equation (1) comes from the vertical Jeans equation for an equilibrium disc. It is therefore essential that the vertical disc scaleheight, h , and the vertical velocity dispersion, σ_z , should refer to the same population of stars. This raises a potential problem.

The dispersion σ_z is usually measured from integrated light spectra near the Mg b lines ($\sim 5150\text{--}5200 \text{ \AA}$), since this region has many absorption lines and the sky is relatively dark. The discs of the gas-rich galaxies for which good $H\text{ I}$ rotation data are available usually have a continuing history of star formation and therefore include a population of young (ages $< 2 \text{ Gyr}$), kinematically cold stars among a population of older, kinematically hotter stars, as we will demonstrate in this paper for the Galactic disc near the sun. The red giants of this mixed young + old population provide most of the absorption line signal that is used for deriving velocity dispersions from the integrated light spectra of galactic discs. These same giants typi-

¹ A maximal disc has the maximum M/L value consistent with the observed rotation curve and a non-hollow dark halo. Typically, the disc of a maximal disc provides about 85 per cent of the rotational velocity at the peak of the rotation curve (Sackett 1997).

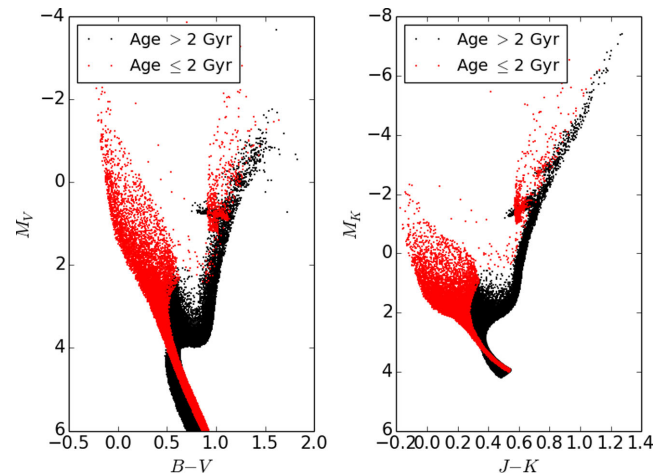


Figure 1. The CMD computed from IAC-STAR for a disc with an exponentially declining star formation law. The red points are stars with ages $\leq 2 \text{ Gyr}$. The left-hand panel shows the CMD in the V band. The right-hand panel shows the CMD in the near-infrared. The old giants are the brightest stars in IR.

cally contribute about half of the light of the V -band integrated light spectra of discs (see appendix). On the other hand, red and near-infrared measurements of the scaleheights of edge-on disc galaxies are dominated by the red giants of the older, kinematically hotter population (see right panel in Fig. 1). The dust layer near the Galactic plane further weights the determination of the scaleheight to the older kinematically hotter population: e.g. de Grijs, Peletier & van der Kruit (1997).

Therefore, in equation (1), we should be using the velocity dispersion of the older disc stars in combination with the scaleheights of this same population for an accurate determination of the surface mass density. In practice, because of limited signal-to-noise ratios for the integrated light spectra of the discs, integrated light measurements of the disc velocity dispersions usually adopt a single kinematical population for the velocity dispersion whereas, ideally, the dispersion of the older stars should be extracted from the composite observed spectrum of the younger and older stars.

Adopting a single kinematical population for a composite kinematical population gives a velocity dispersion that is smaller than the velocity dispersion of the old disc giants (for which the scale height was measured), and hence underestimates the surface density of the disc. A maximal disc will then appear submaximal. This problem potentially affects the usual dynamical tracers of the disc surface density in external galaxies, like red giants and planetary nebulae, which have progenitors covering a wide range of ages. It therefore affects most of the previous studies. Flynn & Fuchs (1994) demonstrated the presence of bright, kinematically colder stars in the solar neighbourhood. They recognized the importance of isolating the old K-giants for dynamical measures of the surface density of the Galactic disc.

Fig. 1 presents a synthetic colour–magnitude diagram computed using IAC-Star (see Aparicio & Gallart 2004) with the Teramo stellar evolution library and the Castelli & Kurucz bolometric correction library, to show the location of the younger and older red giants. The adopted star formation history has the exponential form $\exp(-t/\beta)$ with $\beta = 20 \text{ Gyr}$. We used a Kroupa IMF and a linear chemical enrichment law, with a mean metallicity $Z = 0.006$ and 0.019 at $t = 0$ and $t = 13 \text{ Gyr}$, respectively. We introduced a spread of $\pm 0.4 \text{ dex}$ in the metallicities at all ages, to match the dispersion

Table 1. Studies that have looked at the solar neighbourhood to estimate the surface density of the Galactic disc and the total surface density (disc + dark halo).

Author	Σ_{disc}	$\Sigma_{\text{total}}(1.1 \text{ kpc})$	Sample
Kuijken & Gilmore (1989a,b,c)	$48 \pm 8 M_{\odot} \text{ pc}^{-2}$	$71 \pm 6 M_{\odot} \text{ pc}^{-2}$	K-dwarfs
Flynn & Fuchs (1994)	$52 \pm 13 M_{\odot} \text{ pc}^{-2}$		K-giants
Holmberg & Flynn (2004)	$56 \pm 6 M_{\odot} \text{ pc}^{-2}$	$74 \pm 6 M_{\odot} \text{ pc}^{-2}$	K-giants
Bovy & Rix (2013)	$38 \pm 4 M_{\odot} \text{ pc}^{-2}$	$68 \pm 4 M_{\odot} \text{ pc}^{-2}$	G-dwarfs

in the observed age–metallicity law in the solar neighbourhood (e.g. Haywood 2008). Stars younger than 2 Gyr are shown in red in Fig. 1 and the black points are for older stars. Fig. 1 shows that the younger giants are more likely to be among the most luminous stars on the giant branch (see appendix for the fraction of total light contributed by the giants). We also show the $M_K, J - K$ colour–magnitude diagram for the same simulation, to indicate the contribution that the older giants make to the near-IR surface brightness in photometric studies of edge-on discs.

1.1 The surface density of the Galactic disc near the sun

So far, we have discussed only the use of integrated light spectroscopy and estimates of the disc scaleheight to measure the surface density of the discs of external galaxies. In the Milky Way, the velocities and spatial distributions of individual tracer stars near the sun can be used for the same purpose. We briefly review the results in Table 1, because they provide a useful context for the integrated light observations of external galaxies.

The values obtained from these different studies agree well. The implications regarding the maximality of the Milky Way’s disc are uncertain, because the radial scalelength of the Galactic disc is not accurately known.

1.2 The Disk Mass Survey

Bershady et al. (2010) used integral field spectroscopy to study the kinematics of stars and gas in the discs of face-on spiral galaxies out to radii of about 2.2 scalelengths. The discs in their sample contribute typically 15–30 per cent of the dynamical mass within 2.2 disc scalelengths, with percentages increasing systematically with luminosity, rotation speed, and redder colour. These trends indicate that the mass ratio of disc-to-total matter remains at or below 50 per cent at 2.2 scalelength, even for the most rapidly rotating discs ($V_{\text{max}} \geq 300 \text{ km s}^{-1}$). The conclusion is that spiral discs are generally submaximal (Bershady et al. 2011). As in all previous dynamical studies of this kind, these authors model the stars in the disc as a single kinematical population and determine a single vertical velocity dispersion to represent all of the stars.

1.3 Are discs really so submaximal?

In the following sections, we analyse the K-giants in the solar neighbourhood, to demonstrate the existence of different populations of stars with different vertical velocity dispersions and discuss the implications for the decomposition of the $H \text{ I}$ rotation curves of external galaxies. While the K-giants dominate the velocity dispersion signal in the integrated spectra of external discs, it is only near the Sun that we can examine in detail the composite kinematical makeup of the K-giant population, and work out the implications for integrated light spectroscopy of an external disc that has a similar star formation history to the Galactic disc near the Sun. In particular,

we would like to evaluate the significance of a cold core of K-giants among the kinematically hotter stars of the old disc.

Section 2 describes our data sample and Section 3 describes the analysis. The results are discussed in Section 4. Section 5 uses the Besançon model as a check on any unanticipated selection effects that our sample of giants may have, Section 6 uses the Besançon model to look at the implications for external galaxies, Section 7 has our conclusions and Section 8 discusses our future plans for this project.

2 SELECTION OF SAMPLE

We would like to construct a sample of nearby red giants that has age and kinematics for each star. Currently, these data are not yet available but are soon expected from asteroseismology of red giants (e.g. Soderblom 2010). At present, guided by Fig. 1, we can use giants of known vertical velocity (W velocity) and absolute magnitude to look at their distribution over kinematics and luminosity. We use two different samples to build up our data set – a sample of K-giants in the South Galactic Pole (SGP), for which the W velocities come mainly from the radial velocities, and giants from the Bright Star Catalog (BSC).

The Flynn & Freeman (1993) sample (hereafter **FF**) is a sample of 560 K-giants at the SGP with $V < 11.0$. It was selected from the following sources.

- (i) Henry Draper (HD) stars with spectral types between G8 and K5, brighter than luminosity class V, from the Michigan Catalog Volumes III and IV (Houk 1982; Houk & Smith-Moore 1988).
- (ii) The Eriksson (1978/1995) sample of SGP stars with $0.95 < B - V < 1.55$ and $V < 11.0$.
- (iii) A sample of fainter giants from the Zeiss 6-inch camera on the Oddie telescope at Mount Stromlo Observatory (see **FF**).

We used a subset of 303 stars from the **FF** sample with measured $B - V$, radial velocity and absolute magnitude (M_V). The absolute magnitudes in the **FF** sample were originally estimated using the intermediate-band photometric David Dunlop Observatory (DDO) system. Holmberg & Flynn (2004) later compared the DDO absolute magnitudes with the more accurate *Hipparcos* absolute magnitudes and found some systematic offsets in the DDO system. The absolute magnitudes of our stars from the **FF** sample were re-calibrated as suggested by Holmberg & Flynn (2004). The expected absolute magnitude of the red giant branch clump stars ($M_V \sim 0.8$) is consistent with the revised magnitude scale.

The sample of 303 **FF** red giant stars with colour, magnitude and radial velocity information is not large enough to evaluate the detailed structure of the W velocity distribution function, so we increased our sample size by adding giants from the BSC (Hoffleit & Jaschek 1991). The BSC is more or less complete to $V = 7$. We chose stars from the BSC that have the same spectral type as the **FF** stars, i.e. from G8III to K5III.

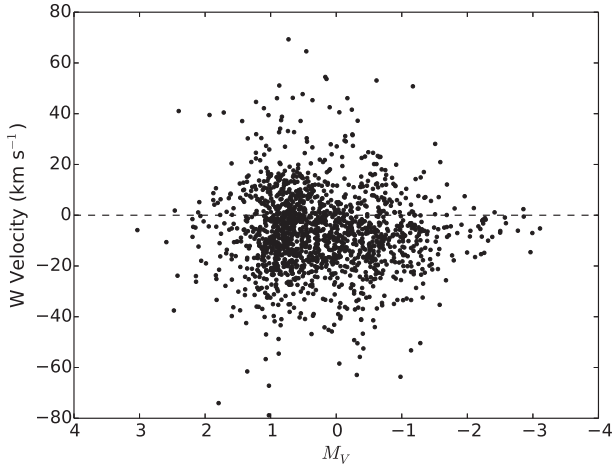


Figure 2. W velocities versus absolute magnitude for the nearby giants. The colder stars with smaller dispersions can be seen at $M_V \leq -2$. The offset from zero of the mean W-velocity is due to 7 km s^{-1} reflex W-motion of the sun.

3 ANALYSIS

In this section, we calculate the space velocities for our sample of stars and represent the distribution of W velocity in terms of different populations of stars.

3.1 Vertical velocities of the sample of giants

Of the above subset of 303 stars from the FF sample, proper motions for 300 are available from the UCAC4 catalogue (Zacharias et al. 2013); 134 of them have parallaxes and associated errors from the extended *Hipparcos* catalogue (Anderson & Francis 2012). Photometric distances for all 300 stars were calculated using the data in FF and the corrected M_V values using the method described by Holmberg & Flynn (2004). The M_V values have errors of 0.35 mag (Holmberg & Flynn 2004) and the apparent V magnitudes in Flynn & Freeman (1993) have typical errors ~ 0.02 mag. Therefore, our photometric distances typically have a 16 per cent error. For the final calculation of W velocities, we compared the relative errors of the data from the *Hipparcos* catalogue (where available) and the photometric distances, and used the distance with the smaller relative error.

The BSC catalogue has radial velocities with typical errors $< 1 \text{ km s}^{-1}$. It also contains the parallaxes and proper motion from the *Hipparcos* catalogue. Our final sample now contains 1740 stars.

The stellar W velocities were calculated as described in Johnson & Soderblom (1987), with the W velocity positive towards the North Galactic Pole. The errors of the W velocities were again calculated as in Johnson & Soderblom (1987). For our study of the W velocity distribution function, only stars with W velocity errors $< 5 \text{ km s}^{-1}$ were retained in the sample to avoid contamination of the velocity distribution by measurement errors. Large errors will compromise our attempt to recover the young component that has small dispersions. Our sample now contains W velocities for 1567 stars. Fig. 2 shows their W velocities against the absolute magnitude, M_V . The W velocities are heliocentric, and the solar motion (our data has mean $W = -7 \text{ km s}^{-1}$) is evident in Fig. 2. The rapid decrease in the stellar density for stars with $M_V > 1$ results from the apparent magnitude and spectral type limits of our sample. The smaller velocity dispersion of the younger disc giants ($M_V < 0$) is

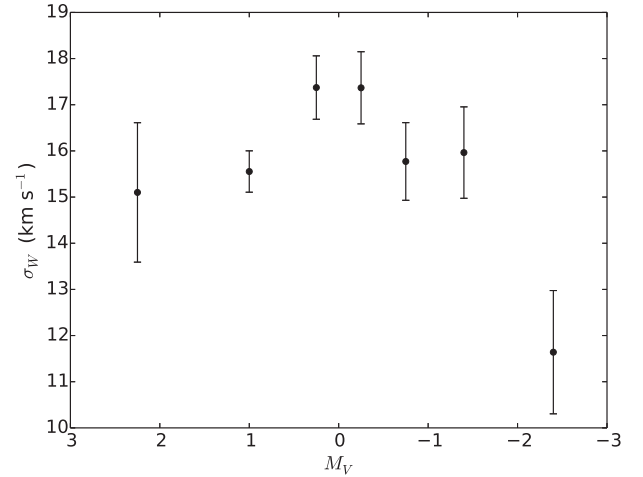


Figure 3. The vertical velocity dispersion (σ_W) versus absolute magnitude for the nearby giants. The brighter stars ($M_V < -2$) are much colder as indicated by their low σ_W value.

also evident (cf. Fig. 1, left panel). The older stars show a visibly larger spread in W velocities. Fig. 3 shows the σ_W versus M_V for our sample. The low dispersion of the colder component at $M_V < -2$ is clearly visible. Flynn & Fuchs (1994) also show the presence of this cold, bright population of stars in the solar neighbourhood.

3.2 Age-velocity relation

It has long been known that the velocity dispersion of stars in the Galactic thin disc near the Sun depends on their age (see e.g. Delhaye 1965 for a summary). The young disc stars with ages < 2 Gyr have $\sigma_W \sim 10\text{--}12 \text{ km s}^{-1}$ and stars older than ~ 2 Gyr have $\sigma_W \sim 20 \text{ km s}^{-1}$. Several more recent works have looked at the structure of the age-velocity relation of thin disc stars and have found similar results (Freeman 1991; Edvardsson et al. 1993; Gomez et al. 1997; Quillen & Garnett 2000): a steady increase in σ_W for stellar ages up to $\sim 2\text{--}3$ Gyr and then a roughly constant velocity dispersion for stars with ages between about 3–10 Gyr. Based on these results, if we were to look at the W velocity distribution of thin disc stars near the sun, we would find that the data could be well represented by two Gaussians – one with a standard deviation of $\sim 10\text{--}12 \text{ km s}^{-1}$ representing the younger stars and the other with a standard deviation of $\sim 20 \text{ km s}^{-1}$ representing the older stars.

Other studies (e.g. Wielen 1977) indicate that the velocity dispersion of the thin disc stars does not plateau for the older stars but continues to increase steadily with age. In their study of the Geneva-Copenhagen sample, Casagrande et al. (2011) find that the velocity dispersion continues to increase up to an age of ~ 10 Gyr. Their derived rate of increase for the dispersion of the older stars depends on the adopted stellar models and the abundance and age cuts imposed on the sample (see their fig. 17). If this continuously rising velocity dispersion with age represents the W velocity distribution of the nearby thin disc, then a simple two-component distribution would not be a good representation of the velocity distribution. A more complex model would be required. For the purpose of this paper, we will adopt the former model, assuming that two approximately Gaussian velocity components (older and younger) are present among the giants of the thin disc.

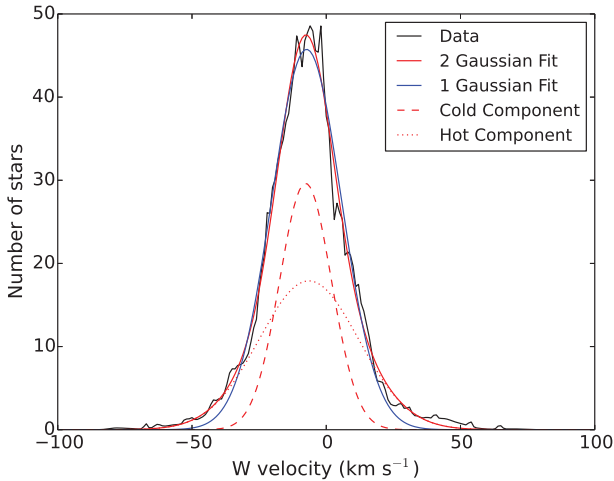


Figure 4. Generalized histogram of W velocities for the combined red giants from Flynn & Freeman (1993) and BSC (in black). The red curve is the best fit to the data, using 2 Gaussians to represent the colder (red dashed line) and hotter (red dotted line) components of the thin disc. The blue curve represents the best single-Gaussian fit, for comparison.

3.3 Multiple populations of stars

Our aim is to determine whether the kinematical parameters for two different population of stars (i.e. the younger, colder population and the older, hotter component) can be extracted from our sample of W velocities of nearby stars. In order to do this, we constructed a generalized histogram of W velocities by representing the velocity of each star as a Gaussian of unit area with mean at its observed W velocity and the error in W velocity as its standard deviation (see Fig. 4). The motivation for using a generalized histogram was to avoid the effects of binning. Our Gaussian models are of the form:

$$\sum_{k=1}^n A_k e^{-(x-\mu_k)^2/2\sigma_k^2}, \quad (2)$$

where A is the amplitude, μ is the mean and σ is the standard deviation of the Gaussian. For a single Gaussian model, $n = 1$ and for a double Gaussian model, $n = 2$.

We used the `curve_fit` module in the `PYTHON SCIPY.OPTIMIZE` package to determine the parameters for the two Gaussians. `Curve_fit` uses non-linear least squares and the Levenberg–Marquardt algorithm. It requires an initial guess of parameters and returns the best-fitting values, along with the covariance matrix. The errors associated with each parameter are the square roots of the corresponding elements on the diagonal of the covariance matrix. To fit a two-Gaussian model, we need to estimate six parameters i.e the amplitude, mean and standard deviation for each component. We will also be fitting single Gaussian models (three parameters) for comparison.

In order to evaluate whether a two-component model is preferred over a one-component model, we compute the Akaike Information Criterion (AIC) which can be used to determine whether adding additional parameters results in a better fit. The AIC is defined by

$$\text{AIC} = n \ln(\text{SSE}) - n \ln(n) + 2p, \quad (3)$$

where n is the number of samples, p is the number of parameters in the model, and SSE is the sum of the squared errors

$$\text{SSE} = \sum (y_{\text{data}} - y_{\text{model}})^2. \quad (4)$$

Table 2. The fit results for the one-component and two-component models. The lower value of the AIC indicates that the two Gaussian model is preferred, despite the larger number of parameters.

	Cold component	Hot component	Single Gaussian fit
Amplitude	29.6 ± 3.1	17.9 ± 3.2	45.7 ± 0.4
Mean (km s^{-1})	-7.7 ± 0.2	-6.5 ± 0.5	-7.3 ± 0.1
Sigma (km s^{-1})	9.6 ± 0.5	18.6 ± 1.0	13.0 ± 0.1
AIC		55.2	155.7

The AIC penalizes additional parameters in the model; the model with the lowest AIC is preferred.

4 THE TWO VELOCITY COMPONENTS

We now derive the double Gaussian and single Gaussian fits to the distribution of W velocities for our sample of K-giants. A significant cold component is visible in the double Gaussian fit. We show again that the brightest giants ($M_V \leq -1.8$) are kinematically very cold, while the fainter giants are an almost homogenous mixture of the hot and cold populations.

Fig. 4 shows the generalized velocity histogram of our sample of stars (black), fit with a two component model (red). It demonstrates the presence of a colder population of stars among a hotter disc population.

The results of our single Gaussian fit and double Gaussian fit are tabulated in Table 2.

Using equation (3), we get an $\text{AIC} = 55.2$ for the two-component model and $\text{AIC} = 155.7$ for the one-component model. Clearly, the two-component model is preferred in this case. Fig. 4 shows the fit to the generalized histogram using two-component and one-component fits. The two-component fit is visibly better than a single Gaussian fit.

The goal is to use the measured velocity dispersion and the scaleheight to calculate the surface density of galactic discs that are viewed more or less face-on. The adopted velocity dispersion and the calculated surface density depend on the kinematical model (one component or two), and we now estimate how much difference this can make. We use equation (1) which relates the surface density Σ , the scaleheight h and the velocity dispersion σ of the disc. The scaleheight cannot be measured directly: it is estimated from the scaling laws for the scaleheight, and pertains to the old disc population, as explained in Section 1. The underlying dynamical assumption is that the disc is in vertical equilibrium in its own gravitational potential, so the scaleheight and the velocity dispersion should be for the same population. What is the effect on the surface density of using a single-component kinematical model to represent the disc, when in reality there are two kinematical components? The true velocity dispersion of the old disc is then the dispersion σ_{hot} of the hotter of the two components, and the true surface density of the disc is $\Sigma_{\text{true}} = f\sigma_{\text{hot}}^2/Gh$. On the other hand, if we were to use a single component kinematical model, we would calculate its surface density as $\Sigma_{\text{single}} = f\sigma_{\text{single}}^2/Gh$. The velocity dispersion σ_{single} for the single-component model is lower than σ_{hot} , as in Table 2 (13.0 and 18.6 km s^{-1} , respectively). The adopted scaleheight h is not affected by the kinematical measurements, so the effect of using the one-component model is to underestimate the surface density of the disc.

Taking, in each case, the same scaleheight h for the old thin disc, the ratio of surface densities derived from using the dispersion for

(a) the hotter component of a double Gaussian fit and (b) a single Gaussian fit is

$$\frac{\Sigma_2}{\Sigma_1} = \frac{\sigma_2^2}{\sigma_1^2} = \frac{(18.6 \pm 1.0)^2}{(13.0 \pm 0.1)^2} = 2.05 \pm 0.16. \quad (5)$$

The subscript 1 refers to the case where we fit a single Gaussian and subscript 2 refers to the hotter (older) component of the double Gaussian fit. If we were using integrated light spectroscopy to measure the surface density of the disc of an external galaxy, in which the star formation history over the last 10 Gyr has been similar to that in the solar neighbourhood, and if we had used a single-component Gaussian velocity distribution instead of deriving the velocity dispersion of the old disc from a two-component velocity distribution, then we would underestimate the surface density of the disc by about a factor 2.

We can use equation (1) and the dispersion for the hotter component of the two-component model in Table 2, to estimate the surface density of the disc near the sun and compare with the more detailed estimates of surface density given in Table 1. We assume that the old disc is vertically exponential, with a scaleheight $h = 300 \pm 50$ pc (e.g. Gilmore & Reid 1983) and a velocity dispersion of $\sigma = 18.6 \pm 1.0$ km s⁻¹ as given in Table 2. The surface density $\Sigma = (2/3\pi)\sigma^2/Gh = 57 \pm 12$ M_⊙ pc⁻², in fair agreement with the range of estimates given for the surface density of the disc in Table 1.

In this section, we have shown that the W velocity distribution of the nearby K-giants is well represented by a two-component distribution. Fig. 3 shows that the more luminous giants have a smaller W velocity dispersion than the fainter giants, and we associate the two components with the older and younger stars of the thin disc.

We can visualize and quantify this effect further, by splitting the sample of stars into three absolute magnitude intervals: $M_V \leq -1.8$, $-1.8 < M_V \leq 0$ and $M_V > 0$. Within each group, the stars are ordered by increasing absolute magnitude. We then form the cumulative sum of $|W - \bar{W}|$ versus the rank of the star, where \bar{W} is the mean value of W for the group. The point of doing this kind of analysis is that, for a group of stars with homogeneous velocity dispersion (not necessarily a single Gaussian component), the plots of the sum of $|W - \bar{W}|$ against rank will be a straight line, and the slope is a measure of the velocity dispersion. Fig. 5 shows the outcome for each of the three absolute magnitude groups.

The red line in each panel of Fig. 5 is a linear fit to the data. The slope of the line = $\sqrt{2/\pi}\sigma$, where σ is the velocity dispersion. Fitting the slope of the line is equivalent to deriving a single dispersion for the velocity distribution of the stars, after setting their mean velocity to zero. The bright giants with $M_V \leq -1.8$ represent mainly the younger and kinematically colder population. Their dispersion is $\sigma = 5.9$ km s⁻¹ which is colder than the value we obtained for the young, cold component in our two-component Gaussian decomposition.

The two panels of fainter stars with $M_V > -1.8$ are mixed populations of stars of all ages, with similar (larger) dispersions. While the brighter stars in the top panel are clearly from a colder population, we conclude from Fig. 5 that the mixtures of hot and cold populations in the two lower panels are fairly similar and do not change much with absolute magnitude, because the two panels are well fitted by straight lines and have similar slopes with dispersions of 15 km s⁻¹.

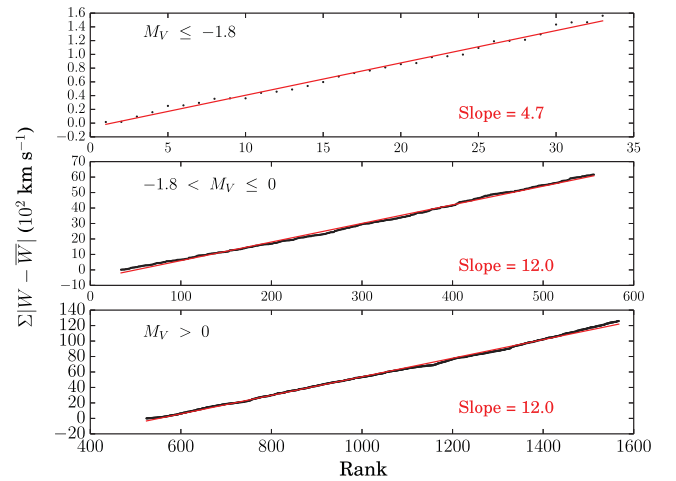


Figure 5. The cumulative sum of $|W - \bar{W}|$ against rank by absolute magnitude in three magnitude intervals for our giants. The x-axis shows the rank of the stars and the y-axis is the cumulative sum of W velocities. See Section 4 in the text for further details. The upper panel is for the bright, young, kinematically colder population. The stars in the two bottom panels contain a mixed population of young and old stars. The velocity dispersion of the population is proportional to the slope of the line.

5 COMPARISON WITH KINEMATICS OF THE BESANÇON MODEL

As a check on what we have learned about the velocity distribution of the nearby thin disc from our sample of nearby giants, we did a similar study on a sample of simulated giants from the on-line Besançon model (Robin et al. 2003). This model was designed to represent the main Galactic structural components and stellar populations. It includes recipes for galactic reddening, the star formation history and the dynamical evolution which manifests as the stellar age-velocity dispersion relation (Robin et al. 2003, Table 4). Our main goal in using the Besançon model here is as a check on any significant unanticipated selection effects in our sample of giants.

Two separate simulated catalogues were generated – one to represent the FF stars and another for the BSC stars. The simulation that mimics the FF giant sample was made by choosing all stars within a distance of 1.5 kpc, $-3 \leq M_V \leq +3$, $-90^\circ \leq b \leq -75^\circ$, $V \leq 11$ and $1.0 \leq B - V \leq 1.5$. This gave ~ 3000 stars. For the BSC giant simulation, we chose stars within a distance of 0.6 kpc, $-3 \leq M_V \leq +3$, $V \leq 7$ and $0.8 \leq B - V \leq 1.8$. No cuts were made in position on the sky. This gave $\sim 10,000$ stars. Fig. 6 compares the luminosity functions of our sample of stars (FF and BSC: upper panel) with the luminosity function of the simulation. The red clump stars ($M_V \sim 0.8$) stand out very clearly in the Besançon model simulation as well as in our sample, as expected. All figures involving the Besançon model in the main body of the paper are using this combined simulated catalogue of the FF and BSC red giants.

Fig. 7 shows the W velocity versus absolute magnitude for the Besançon sample of stars. As in Fig. 2, a kinematically colder component of bright giants can be clearly seen at $M_V < -2$. A small number of high-velocity thick disc stars are present for $M_V > -2$. Fig. 8 is similar to Fig. 3 but for the Besançon sample of stars.

Fig. 9 is similar to Fig. 5 but for the Besançon simulation. As before, the brightest stars correspond to the kinematically cold component. The slope of the linear fit corresponds to a velocity dispersion $\sigma = 7.9$ km s⁻¹ for the stars with $M_V \leq -1.8$. The two panels

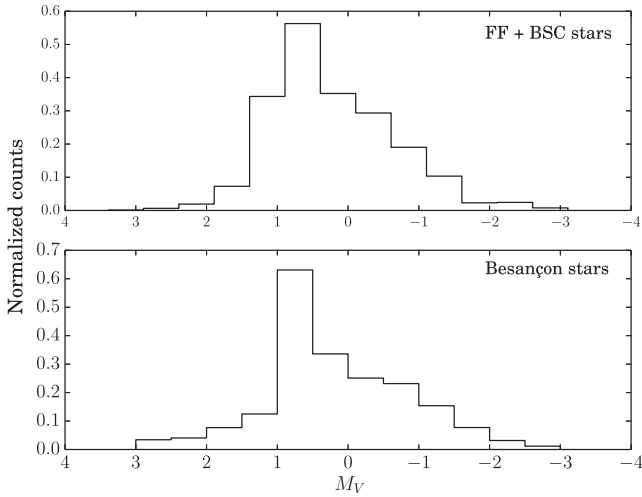


Figure 6. Comparison of the luminosity functions of our sample of stars with a simulation of these stars from the Besançon model. There seems to be a larger fraction of stars with $M_V \sim 1$ in our sample, but otherwise the two samples are a good match.

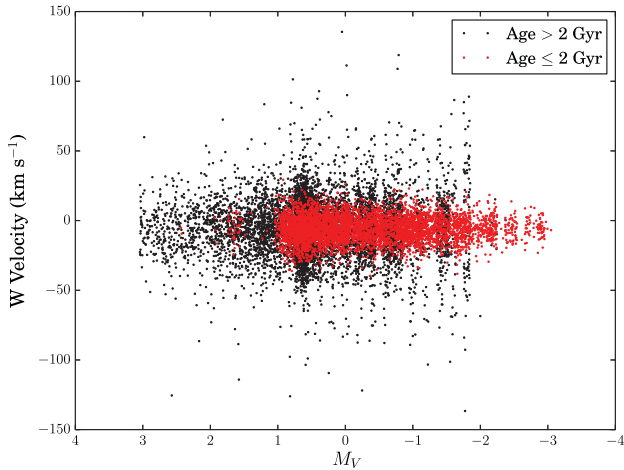


Figure 7. Besançon stars. Stars with $M_V \leq -2$ is comprised purely of the young population. A mixed population of young and old stars can be at $-2 < M_V \leq -1$.

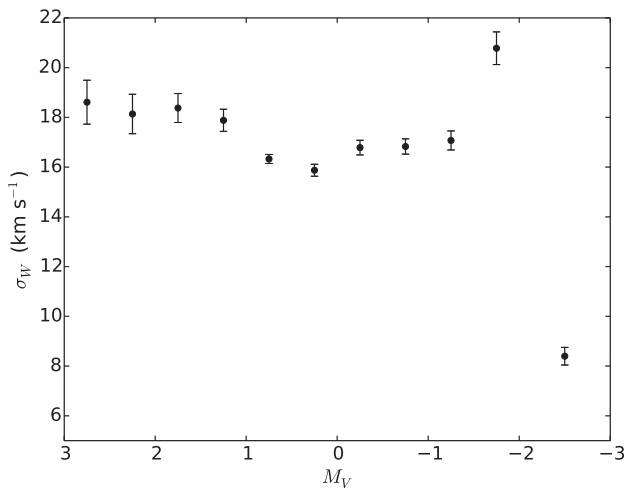


Figure 8. The vertical velocity dispersion (σ_W) versus absolute magnitude for the Besançon sample. The brighter stars ($M_V < -2$) are much colder as indicated by their low σ_W value.

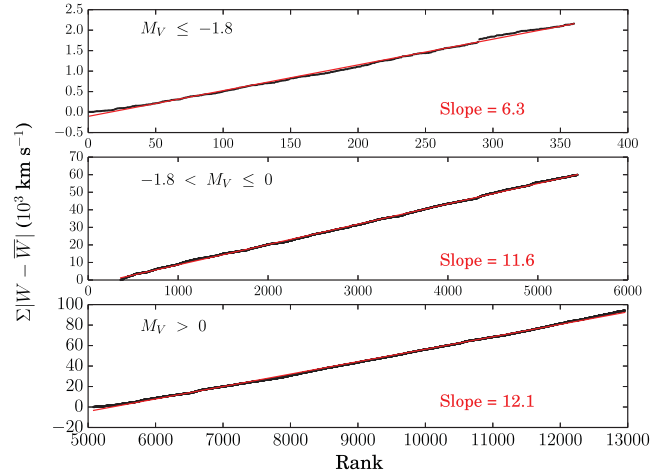


Figure 9. The cumulative W velocities in different magnitude ranges of the Besançon simulation. The x -axis shows the rank of the stars and the y -axis is the sum of modulus of $W - \bar{W}$ velocities. See the text for further details.

Table 3. The fit results for the one component and two component models for the Besançon sample of stars.

	Cold component	Hot component	Single Gaussian fit
Amplitude	264.3 ± 3.8	148.0 ± 4.0	394.4 ± 1.5
Mean (km s^{-1})	-5.64 ± 0.03	-6.26 ± 0.08	-5.82 ± 0.05
Sigma (km s^{-1})	8.95 ± 0.07	18.45 ± 0.17	13.0 ± 0.1

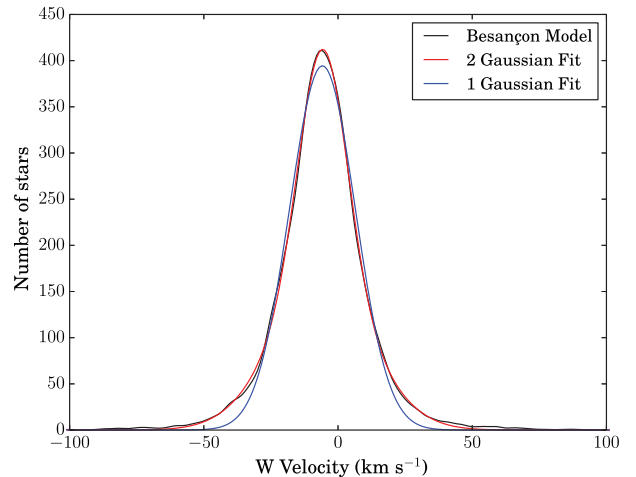


Figure 10. Generalized histogram representing the stars simulated using the Besançon model. The black curve shows the histogram and the red curve is the two-component fit.

of stars with $M_V > -1.8$ contain stars of all ages and have again similar larger dispersions.

We made a similar analysis to that shown in Fig. 4, using the W velocities from the Besançon simulations to create a generalized histogram of velocities, and adopting a velocity error of 2 km s^{-1} for each star. The results are tabulated in Table 3.

Fig. 10 shows the velocity distribution for the Besançon simulation fit with a double Gaussian model and with a single Gaussian model. Clearly, the double Gaussian is a better fit to the data.

The Besançon simulation is a good match to the kinematics of our sample of nearby giants. The two-component dispersion values are very similar to the values obtained for the FF + BSC stars. The

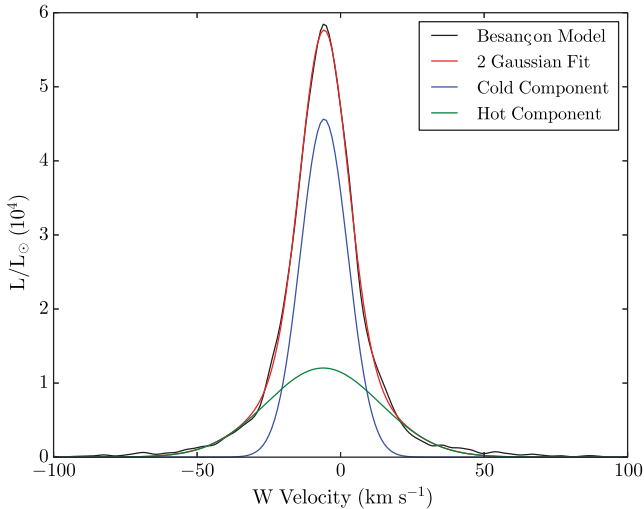


Figure 11. Generalized histogram of the W-distribution of the stars from the Besançon model. Each star contributed a Gaussian with area proportional to its luminosity and dispersion of 2 km s^{-1} . The red curve is the two component fit to the Besançon sample in black. The younger component and the older component are shown in blue and green respectively.

Table 4. Results of the Gaussian fit for the luminosity weighted generalized histogram of the Besançon sample of stars.

	Cold component	Hot component	Single Gaussian fit
Amplitude	45700 ± 400	12000 ± 500	55500 ± 300
Mean (km s^{-1})	-5.73 ± 0.03	-6.078 ± 0.16	-5.788 ± 0.062
Sigma (km s^{-1})	8.23 ± 0.05	19.79 ± 0.30	10.265 ± 0.062

relative numbers of stars in the two components can be calculated from the ratio of the product of the amplitude and dispersion $A\sigma$ for the two components (see equation 2): the ratio of hot:cold stars is about 1.2:1 in both the FF + BSC sample and in the Besançon simulation.

In evaluating the contribution of the kinematically cold component to the integrated light spectrum of a disc with a star formation history like that of the solar neighbourhood, it would be useful to know the ratio of the relative contributions of the colder and hotter components to the surface brightness of the disc. This would allow us to evaluate how much each component contributes to the integrated light of the disc. To estimate this ratio, we built up another velocity histogram using the Besançon model, but this time each star was represented as a Gaussian with area proportional to its luminosity. This histogram, shown in Fig. 11, is then a luminosity-weighted velocity distribution. The luminosity of each star was calculated from its M_V value in the Besançon simulation of the FF and BSC catalogues described earlier in this section. As before, we fit two Gaussians to the generalized histogram. The fit results are shown in Table 4.

The total luminosity of each component is again proportional to the product $A\sigma$. Although the colder stars are fewer in number than the hotter stars, we find that their luminosity is a factor of 1.58 ± 0.06 higher than for the hotter stars. This younger and kinematically colder component would thus dominate the integrated light of a disc galaxy for which the star formation history of the thin disc was similar to that adopted in the Besançon model. We also tried to use similar methods to obtain the luminosity ratio of the kinematically cold/hot stars from our sample (FF & BSC) of stars but, with the

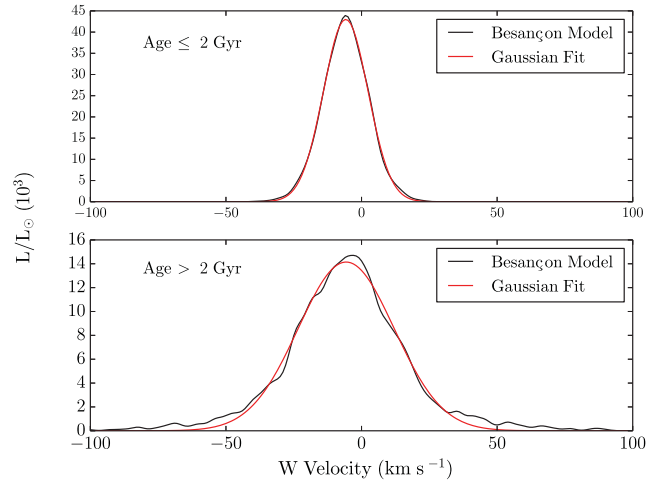


Figure 12. Generalized luminosity histogram of the W-distribution of the stars from the Besançon model based on age. The upper panel has all stars of age $\leq 2 \text{ Gyr}$. These stars contribute the colder component with a narrow σ_W . The bottom panel shows the older stars that can be represented with a Gaussian with larger $\sigma \sim 18 \text{ km s}^{-1}$.

luminosity weighting and the small sample size, we were not able to recover the older disc component of stars. The order of magnitude larger sample size of the Besançon simulation allowed us to derive the luminosity ratio without difficulty.

Fig. 12 shows the Besançon stars split by age into two samples. The young stars (age $\leq 2 \text{ Gyr}$) have a small dispersion of $8.238 \pm 0.013 \text{ km s}^{-1}$ and the older stars have a larger dispersion of $17.695 \pm 0.096 \text{ km s}^{-1}$, as expected.

6 IMPLICATIONS FOR EXTERNAL GALAXIES

The Besançon simulations in the previous section looked at stars in a cone. In order to mimic observing the velocity distribution in external galaxies, we need a sample of stars in a cylinder perpendicular to the plane of the disc. We used the Besançon model to choose giants with spectral type G8III - K5III in the entire simulated sky, with $-3 \leq M_V \leq +3$ and $0.8 \leq B - V \leq 1.8$, within a distance of 5 kpc. We then selected giants in a cylinder of radius 2 kpc. This sample would be similar to what we would observe in the disc of a face-on galaxy from afar.

Fitting a double and single Gaussian to the luminosity weighted velocity histogram of these sample of stars give us the results shown in Table 5. The fit is shown in Fig. 13.

Using an analysis similar to that in Section 5, we find that the ratio of the estimated surface mass density of the disc between using the dispersion of the hotter thin disc component and using the dispersion for the single Gaussian fit is

$$\frac{\Sigma_2}{\Sigma_1} = \frac{\sigma_2^2}{\sigma_1^2} = \frac{(23.9 \pm 0.3)^2}{(15.40 \pm 0.05)^2} = 2.41 \pm 0.06. \quad (6)$$

Table 5. Gaussian fit to the luminosity-weighted histogram of the Besançon sample of stars in a cylinder.

	Cold component	Hot component	Single Gaussian fit
Amplitude ($\times 10^3$)	2050 ± 26	650 ± 27	2633 ± 7
Mean (km s^{-1})	-5.96 ± 0.03	-5.81 ± 0.11	-5.93 ± 0.05
Sigma (km s^{-1})	13.0 ± 0.07	23.90 ± 0.30	15.40 ± 0.05

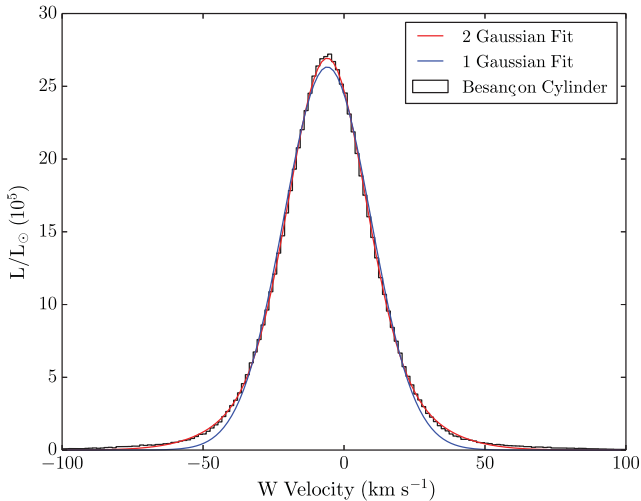


Figure 13. Luminosity-weighted histogram of the W-distribution of the stars from the Besançon stars in a cylinder. The double Gaussian fit is visibly better than the single Gaussian fit.

Table 6. Results of the Gaussian fit for the luminosity-weighted histogram of the Besançon sample of stars in a cylinder with different star formation histories.

	No star formation over last Gyr σ (km s ⁻¹)	Half the star formation over last Gyr σ (km s ⁻¹)
Cold component	14.06 ± 0.05	13.56 ± 0.06
Hot component	27.74 ± 0.36	25.70 ± 0.33
Single Gaussian fit	15.79 ± 0.05	15.61 ± 0.05

As before, the subscript 1 refers to the single Gaussian fit and subscript 2 refers to the hotter (older) component of the double Gaussian fit. The underestimation of the disc surface mass density in the cylindrical geometry is similar to the value that we got for our nearby sample of stars (see Section 4).

The velocity dispersions that we calculated above are appropriate to a region with a similar star formation history and dynamical history to the solar neighbourhood. To get an idea of how the dispersions of the various components would change with a different star formation history, we constructed two different samples of stars: one with half the star formation rate over the last Gyr, and one with no star formation over the last Gyr. We again used a luminosity-weighted histogram to determine how the vertical velocity dispersions of the different Gaussian components would change. Our results are tabulated in Table 6. Although the hot and cold components become slightly hotter as the recent star formation rate decreases, the dispersions for the single Gaussian fits change very little with the change in star formation history. This reflects the age velocity relation adopted in the Besançon model.

7 CONCLUSIONS

Our analysis of W velocities of red giants in the solar neighbourhood shows the presence of two different population of stars – a kinematically hotter component with a dispersion of 18.6 ± 1.0 km s⁻¹ and a kinematically colder component with a dispersion of 9.6 ± 0.5 km s⁻¹. By number, the ratio of hot to cold stars in the solar neighbourhood is about 1.2:1, but this ratio would depend on the star formation history and dynamical evolution of the particular region that is under investigation. We note that the outcome of a simulated

sample from the Besançon model, using similar selection criteria, is an excellent match to our stars both in the velocity dispersions and the ratios of hot to cold stars.

If we were to regard the giants as a single kinematically homogeneous population, and if we further assumed that the scaleheight of this population is the scaleheight derived statistically for the old disc of the galaxy, then we would underestimate the surface mass density of the disc by a factor of 2.05 ± 0.16 (Section 4). We get a similar value of 2.41 ± 0.06 when looking at stars in a cylinder in the Besançon model (Section 6). These assumptions are usually made in making kinematical estimates of the surface density of external disc galaxies. Again, this underestimate of a factor of 2 is appropriate for a region of a disc galaxy which has a similar star formation history and dynamical history to the Galactic disc near the sun. Using a velocity dispersion of 18.6 km s⁻¹ and a scaleheight from literature, we obtain a disc surface density $\Sigma = 57 \pm 12$ M_⊙ pc⁻², which is in fair agreement with the range of estimates calculated for the Milky Way in previous studies, using alternative techniques.

This work demonstrates an issue for studies that use the velocity dispersion of stars in the disc of external near-face-on galaxies to estimate their surface mass density. The scaleheight for these galaxies come from red or near-infrared photometry that is sensitive to the kinematically hotter population of disc stars. On the other hand, the integrated light spectroscopy that is used to estimate the vertical velocity dispersions includes contributions from both younger and older populations of star. We have shown that the contribution of the kinematically colder stars to the integrated light of the solar neighbourhood may significantly outweigh the contribution from the kinematically hotter old disc, by a factor of about 1.56 in surface brightness. This factor is about 1.7 for the cylindrical sample from the Besançon model (Section 6). The outcome would be a significant underestimate of the velocity dispersion of the old disc, and hence of the surface density of the disc. Thus, a maximal disc would appear submaximal, and its dark halo will appear to have a shorter scalelength and higher central density than its true value.

We can illustrate this effect quantitatively with a decomposition of the rotation curve of the spiral galaxy NGC 3198 which was studied in detail by van Albada et al. (1985). The upper panel of Fig. 14 shows a maximum disc decomposition similar to that shown in fig. 4 of van Albada et al. (1985). We have used the disc model of van Albada et al. (1985) and the widely used pseudo-isothermal-sphere (PITS) dark halo model with

$$\rho(r)/\rho(0) = [1 + (r/a)^2]^{-1}$$

for consistency with later work such as Kormendy & Freeman (2014). The rotation curve for the PITS dark halo model has the form

$$V_c^2(r) = V_\infty^2 [1 - (\tan^{-1} x)/x],$$

where $V_\infty^2 = 4\pi G \rho(0) a^2$ and $x = r/a$. The adopted dark halo model parameters for the maximum disc decomposition are: $a = 7.45$ kpc, $V_\infty = 161$ km s⁻¹ and a central density $\rho(0) = 0.0086$ M_⊙ pc⁻³. Although our dark halo model is slightly different from the model used by van Albada et al. (1985, both have constant density central cores), the halo V_c curves are almost identical. The lower panel of Fig. 14 shows the decomposition for a disc surface density that is lower by a factor 2 than the one shown in the upper panel. This decomposition and the maximum disc decomposition are equally satisfactory, illustrating the disc–halo degeneracy, but the amplitude of the rotation contribution for the disc is now lower by $\sqrt{2}$ and the required halo has a much shorter scalelength a and higher central density $\rho(0)$. The halo model shown in the lower panel of Fig. 14

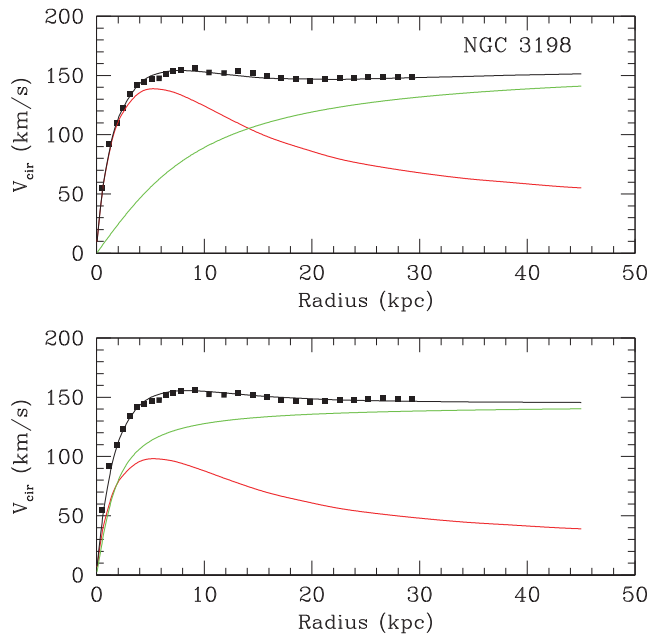


Figure 14. Upper panel shows a maximum disc decomposition of the rotation curve of NGC 3198. Rotation data (black squares) and the rotation curve for the maximum disc (red curve) are adapted from van Albada et al. (1985). The green curve shows the rotation curve for the required halo, and the black curve is the total rotation curve from disc + halo (see Section 7 for details). Lower panel shows the decomposition for a disc with surface density = 0.5 of the maximum disc value. The required dark halo is now much more compact: its central density is about 20 times higher than for the maximum disc decomposition and its scalelength is about five times shorter.

has $a = 1.5$ kpc, $V_\infty = 144$ km s $^{-1}$ and $\rho(0) = 0.17 M_\odot$ pc $^{-3}$. In summary, if a disc of a galaxy like NGC 3198 is truly maximal and its surface density is underestimated by a factor of 2, as we believe could follow from adopting a single velocity dispersion for the young and old giants, then the central density of its dark halo would be overestimated by a factor of about 20 and its scalelength a would be underestimated by a factor of about 5. This would introduce a serious distortion into the scaling laws for dark haloes (see e.g. Kormendy & Freeman 2014).

8 FUTURE WORK

In order to handle the problem of kinematical inhomogeneity described here, we are undertaking a programme to measure the velocity dispersion of the old discs of several large nearby disc galaxies, by making (i) a two-component analysis of the integrated light spectra of regions in their discs, and (ii) measuring radial velocities for large numbers of planetary nebulae in their discs. As for the red giants, the planetary nebulae have progenitors of a wide range of ages, and we can expect them to include kinematically hot and cold subcomponents. The primary outcome will be improved surface densities of the stellar discs, which will then be used to constrain the decomposition of the H I rotation curves into contributions from the disc and the dark halo.

ACKNOWLEDGEMENTS

The authors would like to thank the referee for useful comments that helped improve this paper. The authors are grateful to Marc Verheijen and Matthew Bershady for helpful discussions. SA would

like to thank ESO for the ESO studentship that supported part of this work. KCF thanks Piet van der Kruit for many discussions on related topics over many years. This work has made use of the Besançon Model and the IAC-STAR Synthetic CMD computation code. IAC-STAR is supported and maintained by the computer division of the Instituto de Astrofísica de Canarias. The work of SA and KCF was partly supported by the Australian Research Council grant DP150104129.

REFERENCES

- Anderson E., Francis C., 2012, *Astron. Lett.*, 38, 331
Aparicio A., Gallart C., 2004, *AJ*, 128, 1465
Bell E. F., de Jong R. S., 2001, *ApJ*, 550, 212
Bershady M. A., Verheijen M. A. W., Swaters R. A., Andersen D. R., Westfall K. B., Martinsson T., 2010, *ApJ*, 716, 198
Bershady M. A., Martinsson T. P. K., Verheijen M. A. W., Westfall K. B., Andersen D. R., Swaters R. A., 2011, *ApJ*, 739, L47
Bottema R., 1997, *A&A*, 328, 517
Bottema R., van der Kruit P. C., Freeman K. C., 1987, *A&A*, 178, 77
Bovy J., Rix H.-W., 2013, *ApJ*, 779, 115
Casagrande L., Schönrich R., Asplund M., Cassisi S., Ramírez I., Meléndez J., Bensby T., Feltzing S., 2011, *A&A*, 530, A138
de Grijs R., Peletier R. F., van der Kruit P. C., 1997, *A&A*, 327, 966
Delhaye J., 1965, *Stars and Stellar Systems*, Vol. 6. Univ. Chicago Press, Chicago, IL
Edvardsson B., Andersen J., Gustafsson B., Lambert D. L., Nissen P. E., Tomkin J., 1993, *A&A*, 275, 101
Eriksson W., 1995, *VizieR Online Data Catalog II/120: Phot and Spectrophot Investigation*, South Gal Pole
Flynn C., Freeman K. C., 1993, *A&AS*, 97, 835
Flynn C., Fuchs B., 1994, *MNRAS*, 270, 471
Flynn C., Holmberg J., Portinari L., Fuchs B., Jahreiß H., 2006, *MNRAS*, 372, 1149
Freeman K. C., 1991, in Sundelius B., ed., *Dynamics of Disc Galaxies*. Reidel, Dordrecht, p. 15
Gilmore G., Reid N., 1983, *MNRAS*, 202, 1025
Gomez A. E., Grenier S., Udry S., Haywood M., Meillon L., Sabas V., Sellier A., Morin D., 1997, in Bonnet R. M. et al., eds, *ESA SP-402: Hipparcos - Venice 97*. ESA, Noordwijk, p. 621
Haywood M., 2008, *MNRAS*, 388, 1175
Herrmann K. A., Ciardullo R., Feldmeier J. J., Vinciguerra M., 2008, *ApJ*, 683, 630
Hoffleit D., Jaschek C., 1991, *The Bright Star Catalogue*. Yale Univ. Observatory, New Haven
Holmberg J., Flynn C., 2004, *MNRAS*, 352, 440
Houk N., 1982, *Michigan Catalogue of Two-Dimensional Spectral Types for the HD Stars, Volume_3, Declinations -40°0 to -26°0*. Univ. Michigan, Ann Arbor, MI
Houk N., Smith-Moore M., 1988, *Michigan Catalogue of Two-Dimensional Spectral Types for the HD Stars, Volume 4, Declinations -26°0 to -12°0*. Univ. Michigan, Ann Arbor, MI
Johnson D. R. H., Soderblom D. R., 1987, *AJ*, 93, 864
Just A., Fuchs B., Jahreiß H., Flynn C., Dettbarn C., Rybizki J., 2015, *MNRAS*, 451, 149
Kormendy J., Freeman K. C., 2014, preprint ([arXiv:1411.2170](https://arxiv.org/abs/1411.2170))
Kregel M., van der Kruit P. C., Freeman K. C., 2005, *MNRAS*, 358, 503
Kuijken K., Gilmore G., 1989a, *MNRAS*, 239, 571
Kuijken K., Gilmore G., 1989b, *MNRAS*, 239, 605
Kuijken K., Gilmore G., 1989c, *MNRAS*, 239, 651
Macciò A. V., Ruchayskiy O., Boyarsky A., Muñoz-Cuartas J. C., 2013, *MNRAS*, 428, 882
Maraston C., 2005, *MNRAS*, 362, 799
Quillen A. C., Garnett D. R., 2000, preprint ([arXiv:astro-ph/0004210](https://arxiv.org/abs/astro-ph/0004210))
Robin A. C., Reylé C., Derrière S., Picaud S., 2003, *A&A*, 409, 523
Sackett P. D., 1997, *ApJ*, 483, 103
Soderblom D. R., 2010, *ARA&A*, 48, 581

- Tully R. B., Fouqué P., 1985, *ApJS*, 58, 67
 van Albada T. S., Bahcall J. N., Begeman K., Sancisi R., 1985, *ApJ*, 295, 305
 van der Kruit P. C., Freeman K. C., 1984, *ApJ*, 278, 81
 van der Kruit P. C., Freeman K. C., 2011, *ARA&A*, 49, 301
 Wielen R., 1977, *A&A*, 60, 263
 Yoachim P., Dalcanton J. J., 2006, *AJ*, 131, 226
 Zacharias N., Finch C. T., Girard T. M., Henden A., Bartlett J. L., Monet D. G., Zacharias M. I., 2013, *AJ*, 145, 44

APPENDIX A: CONTRIBUTION OF DIFFERENT PARTS OF THE CMD TO THE INTEGRATED SPECTRA OF THE DISC

The Galactic disc near the sun is a composite population, with stars covering the whole range of age from very young to about 10 Gyr. The stellar population is similarly composite in other star-forming galaxies; the details depend on the local star formation history. As a guide to the relative contributions to the integrated light in external galaxies, from young and old giants, bright main-sequence stars, and the main-sequence below the old turnoff, we use the IAC-STAR synthetic CMD computation code to evaluate the contributions from the different parts of the CMD to the integrated light of the disc for a star formation history like that described in Section 1 (see Fig. 1 and related text). The region of the spectrum that is mostly used for integrated light spectroscopy of the disc is around 5200Å near the Mg b band. We are therefore interested in the relative contributions to the integrated light at the V band.

Fig. 1 illustrates the regions of the CMD that are populated by younger and older stars. We partition the CMD somewhat arbitrarily into three regions: the bright main sequence ($M_V \leq 4$, $B - V \leq 0.7$), the lower main sequence ($M_V > 4$) and the red giants ($M_V \leq 4$, $B - V > 0.7$). For each of these three regions of the CMD, we constructed the M_V luminosity function for the stars in the IAC simulated catalogue. For the adopted star formation history ($\propto \exp(-t/\beta)$ with $\beta = 20$ Gyr), the contributions from the three regions to the V-band light are: bright main sequence 37 per cent, lower main sequence 10 per cent and red giants 53 per cent. The young giants (age ≤ 2 Gyr) contributed 16 per cent of the total light, and the older giants contributed 37 per cent of the total light. These relative contributions depend on the adopted star formation history. For a more nearly constant star formation history, with $\beta = 60$ Gyr, the younger and older giants contribute 16 and 32 per cent, respectively, to the integrated light.

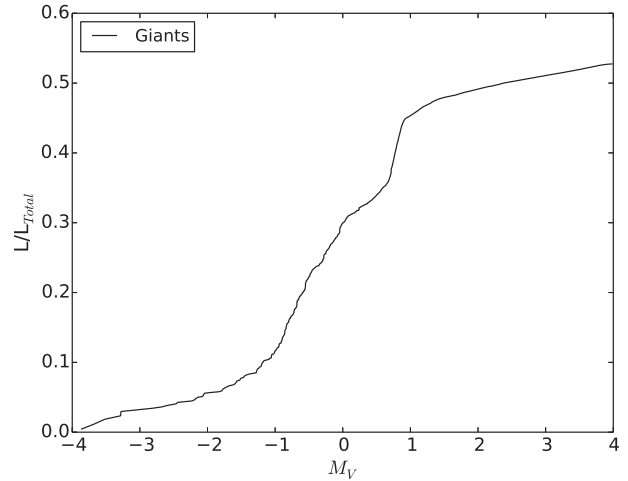


Figure A1. Cumulative histogram of the integrated light of red giants derived from the IAC-STAR simulation. L_{total} is the total light from all stars. The giants provide about 53 per cent of the total surface brightness of the disc, for the adopted star formation history $\beta = 20$ Gyr.

Although the spectra of stars around the main-sequence turnoff do contribute to the equivalent widths of the absorption lines in the Mg b region, the red giants are the main contributors to the absorption lines in the integrated spectra from which the velocity dispersions are measured. This is why we chose to concentrate on the kinematics of the red giants in the solar neighbourhood in this paper. Comparison of the integrated spectra of galactic discs with the spectra of individual giant stars shows that the lines of the integrated spectra are diluted by the contribution of continuum light from the hotter main-sequence stars.

The young giants contribute 30–35 per cent of the total light from the giants. The point of this paper is that the contribution from these stars needs to be taken into account when measuring the velocity dispersion from the integrated light of external galaxies, to avoid underestimating the surface mass density of the galactic disc.

This paper has been typeset from a $\text{\TeX}/\text{\LaTeX}$ file prepared by the author.